Modeling Silicon CMOS devices for quantum computing

Benjamin Venitucci
Univ. Grenoble Alpes, CEA, IRIG
MEM/L_Sim
Grenoble, France

Jing Li
Univ. Grenoble Alpes, CEA, IRIG
MEM/L_Sim
Grenoble, France

Léo Bourdet
Univ. Grenoble Alpes, CEA, IRIG
MEM/L_Sim
Grenoble, France

Yann-Michel Niquet
Univ. Grenoble Alpes, CEA, IRIG
MEM/L_Sim
Grenoble, France
yniquet@cea.fr

***Abstract* — We review our recent results on the modeling of silicon spin qubits. We describe, in particular, the methodology we have set-up for the simulation of these devices, and give some illustrations on silicon-on-insulator (SOI) qubits. We discuss, in particular, the electrical manipulation of electron and hole spins.**

Keywords—Modeling, spin quantum bits, silicon, quantum information.

I. Introduction

A quantum bit (qubit) is a device where an information is stored as a coherent superposition $|\psi\rangle = \alpha|0\rangle + \beta|1\rangle$ of two quantum states $|0\rangle$ and $|1\rangle$ (for example, two spin states $|0\rangle \equiv |\downarrow\rangle$, $|1\rangle \equiv |\uparrow\rangle$). Such devices open new perspectives for information processing, thanks, e.g., to the intrinsic parallelism afforded by the superposition of inputs/outputs. Protecting this superposition from decoherence and relaxation (drifts in α, β due to noise and unwanted interactions) is, however, one tremendous challenge (among others) [1].

The spins of electrons confined in semiconductor quantum dots (QDs) actually make promising solid-state qubits with good prospects for large scale integration [2, 3]. High fidelity single and two qubits gates have been demonstrated in III-V materials as well as in silicon [4, 5, 6, 7]. Silicon is an attractive material for quantum information devices because the majority ^{28}Si isotope has no nuclear spin, effectively decoupling electron and hole spins from the lattice and allowing for longer coherence times [8]. Also, silicon benefits from the strong portfolio of technologies developed in conventional micro-electronics for the design of complex and scalable devices.

Many aspects of the physics of silicon qubits are, however, still poorly understood. It is, therefore, essential to complement the experimental activity with microscopic modeling able to give insights into the operation of these devices and provide guidelines for their optimization.

In this paper, we review the methodology we have set-up for the modeling of spin qubits in semiconductors. We then discuss some applications to electron and hole qubits in silicon-on-insulator (SOI) devices. We first give a short introduction to these devices (section II), then outline the modeling methodology (section III), and discuss the manipulation of spin qubits as an illustration (section IV).

II. Spin qubits on SOI

We focus on the SOI devices fabricated in Grenoble as an illustration (Fig. 1). The layout of these devices resembles conventional silicon nanowire Trigate MOSFETs [9, 10, 11]. Thanks to larger source/gate and gate/drain spacers, the devices go into the Coulomb blockade regime at low temperature: quantum dots form under the gates, in which the number of carriers can be controlled by the bias voltages. The information is then stored in the spin of the carrier(s) trapped under the gates. For that purpose, the $|\uparrow\rangle$ and $|\downarrow\rangle$ spin states are split by a static magnetic field **B**. This Zeeman splitting $\Delta E = g\mu_B B$ (where $g \simeq 2$ and μ_B is Bohr's magneton) is typically of the order of a few tens of μeV, which is one of the reasons why the devices must be operated at very low temperatures (< 100 mK).

The spin can then be manipulated by radio-frequency (RF) bursts on the gates, resonant with the Zeeman splitting between the up and down spins ($\Delta E \simeq 40$ μeV $\Rightarrow$ frequency $f_L \simeq 10$ GHz). Coherent photon absorption and stimulated emission indeed drive rotations of the spin called "Rabi oscillations". Starting from the ground-state $|\downarrow\rangle$, any superposition $|\psi\rangle = \alpha|\downarrow\rangle + \beta|\uparrow\rangle$ can in principle be reached that way. The number of spin rotations per unit of time is characterized by the Rabi frequency $f_R << f_L$ (typically 1 to 100 MHz). Note that the spin must be coupled to the orbital motion of the carrier under the gate by spin-orbit coupling (SOC) in order to be manipulated with a RF electric field. SOC is, however, known to be very weak in the conduction band of silicon. Alternatively, the spin can be manipulated with the RF magnetic field produced by a nearby current line.

The second dot on Fig. 1 is used to measure the spin in the qubit through "Pauli spin blockade": The source-drain current is indeed blocked when the spins in the two dots are parallel ("triplet" state) because the carriers can not tunnel from one dot to the other ("two carriers with same spin can not occupy the same level"). More complex one and two-dimensional layouts (bearing less resemblance to traditional MOSFETs) have been designed in order to allow for more versatile interactions between qubits (two qubit gates). These interactions are controlled by inter-dot tunneling and Coulomb repulsion, which translate into an effective "exchange" interaction between spins.

978-1-7281-0940-4/19/$31.00 ©2019 IEEE

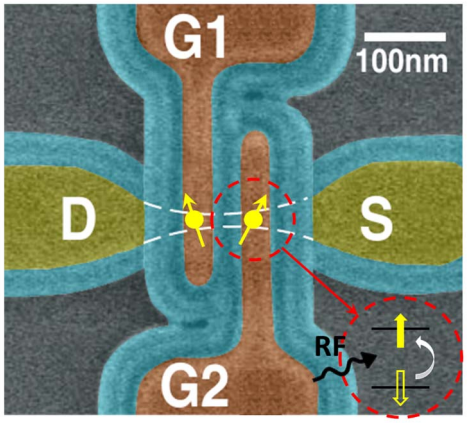

Fig. 1: SEM image of a SOI device. The gates G1 and G2 control two quantum dots along a [110] Si nanowire (outlined by the dashed white lines). The dot under G1 is used as a filter to measure the spin in the qubit under G2 through Pauli spin blockade of the source-drain (S-D) current (current blocked when spins parallel). The electronic structure of the qubit is depicted in the inset. The information is encoded as a superposition of the up and down spin states split by a static magnetic field. The qubit is manipulated by radio-frequency pulses on G2, resonant with the splitting between the two spin levels. Adapted from [10].

III. Methods

We have developped a specific methodology for the microscopic modeling of spin qubit devices (Fig. 2).

The potential landscape in the devices is first computed in the empty dots with a finite volumes Poisson solver. Screening by source/drain reservoirs can be taken into account at this stage with semi-classical approximations for the electron/hole carrier density in the contacts.

Then, N single-particle states $|\varphi_i\rangle$ are calculated in this potential using either a multi-bands **k.p** or a tight-binding (TB) model [11, 12, 13]. TB captures the multi-valley character of the conduction band of silicon and SOC at the atomistic level. It can also describe atomic scale features such as surface roughness and impurities. It is, therefore, ideally suited to the microscopic modeling of qubits. Its numerical cost scales, however, at least linearly with the number of atoms. **k.p** calculations are, therefore, more suitable for large scale systems and hole qubits where the description of SOC is simpler (using either four or six bands **k.p** models). There also exists a four bands **k.p** model accounting for SOC in the conduction band [14]. The set of differential equations for the **k.p** envelope functions is discretized over a finite differences mesh. The matrices of relevant observables (such as spin, gate potentials, etc...) are then computed within the basis of the N $|\varphi_i\rangle$'s. These matrices can later be used to build effective, low-energy Hamiltonians for the qubits.

As an illustration, the 3D model of an electron spin qubit in a silicon nanowire controlled by a partially overlapping gate is shown in Fig. 3. The location of the electron trapped under this gate is outlined in orange; the squared TB wave function of the ground-state is plotted in a transverse cross section in the inset. The electrons (and holes) tend to localize in the corner(s) covered by the gate [15], where the electric field is maximum. These devices, therefore, form low symmetry-dots, which tends to enhance SOC [11, 16].

The many-electron states relevant for the modeling of multiply-charged dots, of Pauli spin blockade readout

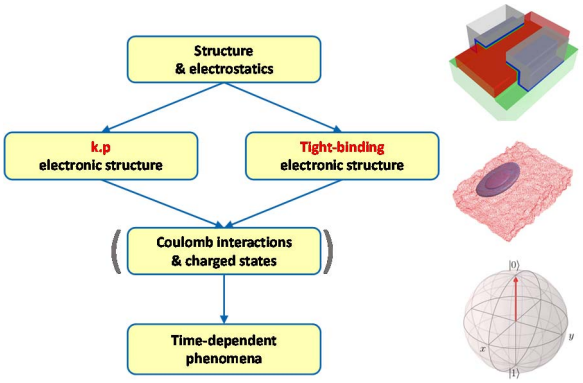

Fig. 2: Computational methodology developed for the qubits.

(singlet/triplet states), and of multi-qubit gates can then be computed with either mean-field approximations (Hartree/Hartree-Fock, usually performed within the reduced basis set of the N precomputed φ_i's), or with a configuration interaction (CI) method [17]. The latter captures the correlations among electrons and is most often the method of choice for the description of the many-electron physics. The principle of CI is to expand the many-particle wave function in a basis of Slater determinants built from a subset of M φ_i's. The basic inputs of CI are the Coulomb integrals:

$$U_{ijkl} = \iint d^3\mathbf{r}\, d^3\mathbf{r}'\, \varphi_i(\mathbf{r})\varphi_j^*(\mathbf{r})\, V(\mathbf{r},\mathbf{r}')\varphi_k^*(\mathbf{r}')\varphi_l(\mathbf{r}') \quad (1)$$

where $V(\mathbf{r},\mathbf{r}')$ is the potential created at point $\mathbf{r}'$ by a charge at point $\mathbf{r}$. These integrals can formally be written as:

$$U_{ijkl} = \int d^3\mathbf{r}\, \rho_{ij}^*(\mathbf{r})\, V_{kl}(\mathbf{r}) \quad (2)$$

where $\rho_{ij}(\mathbf{r}) = \varphi_i^*(\mathbf{r})\varphi_j(\mathbf{r})$ is a joint density and $V_{kl}(\mathbf{r})$ is the potential created by the joint density $\rho_{kl}(\mathbf{r})$. The latter is obtained from the finite volumes Poisson solver using this (possibly complex) joint density as input. The calculation of these integrals may be the most time-consuming part of the simulation. It can, however, be efficiently distributed over a large number of cores on a high-performance parallel cluster. The solution of Poisson and **k.p** equations as well as the

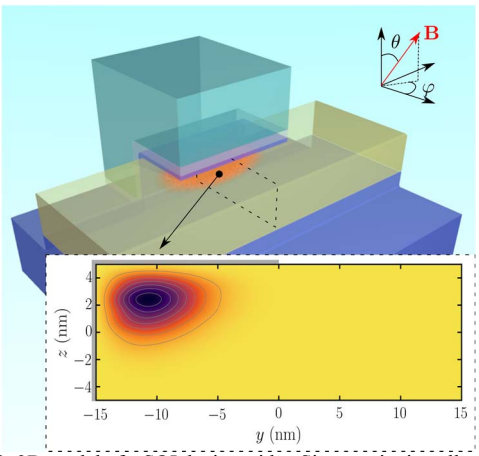

Figure 3: 3D model of a SOI device with a Si nanowire in yellow (cross section 30 nm × 10 nm), SiO_2 in dark blue, and a partly overlapping, 30 nm long gate in light blue. The location of the electron trapped under the gate is sketched in orange. A map of the squared TB wave function is plotted in the cross-section outlined by the dashed black lines. The orientation of the magnetic field **B** (see Fig. 6) is characterized by the angles θ and φ.

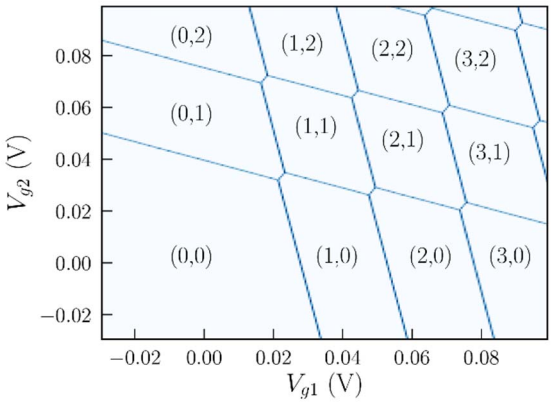

Figure 4: Stability diagram computed for a "double dot" system similar to Fig. 1. The number of electrons (n_1, n_2) in dots 1 and 2 is given as a function of the gates voltages V_{g1} and V_{g2}. Such maps can be reconstructed from the charging energies computed with CI.

calculation of the U_{ijkl}'s are actually parallelized within a mixed OpenMP+MPI scheme. The M φ_i's used to build the CI determinants may be pre-optimized with Hatree-Fock and the basis set of CI determinants filtered out in order to further speed-up the calculation.

As an illustration, the stability diagram computed for a "double dot" system similar to Fig. 1 is plotted in Fig. 4. This map gives the number of electrons (n_1, n_2) in dots 1 and 2 as a function of the gates voltages V_{g1} and V_{g2}. It is used to find the relevant operating points for the qubits (dot filling, control of tunneling, etc...). The stability diagram can be constructed from the intra- and inter-dot charging energies extracted from the CI calculations.

Finally, the response of the system to various control signals and perturbations can be analyzed with a time-dependent solver. For that purpose, the time-dependent Schrödinger equation $[H_0 + V(t)]|\psi(t)\rangle = i\hbar\,\partial|\psi(t)\rangle/\partial t$ is solved in a basis set of eigenstates of the "static" single- or many-particle Hamiltonian H_0. The evolution operator between two time steps t and t+dt is expanded as a Chebyshev polynomial [16, 18] of the Hamiltonian $H(t) = H_0 + V(t)$. Single/two-qubit gate operations and decoherence can be completely simulated in this framework starting from a microscopic (atomic scale) geometry, possibly including disorder (e.g., roughness and charged traps [16, 19]).

Such microscopic simulations can also provide valuable input parameters for the modeling of large scale arrays of qubits using effective Hamiltonians [20].

IV. Applications

We now discuss two applications dealing with the electrical manipulation of electron and hole spin qubits.

A. Electron spin qubits.

SOC is known to be small at the conduction band edge of silicon, partly due to the indirect nature of the bandgap. On the one hand, this effectively decouples the electron spins from electrical and charge noise as well as phonons, hence enhances spin lifetimes. On the other hand, this prevents the direct

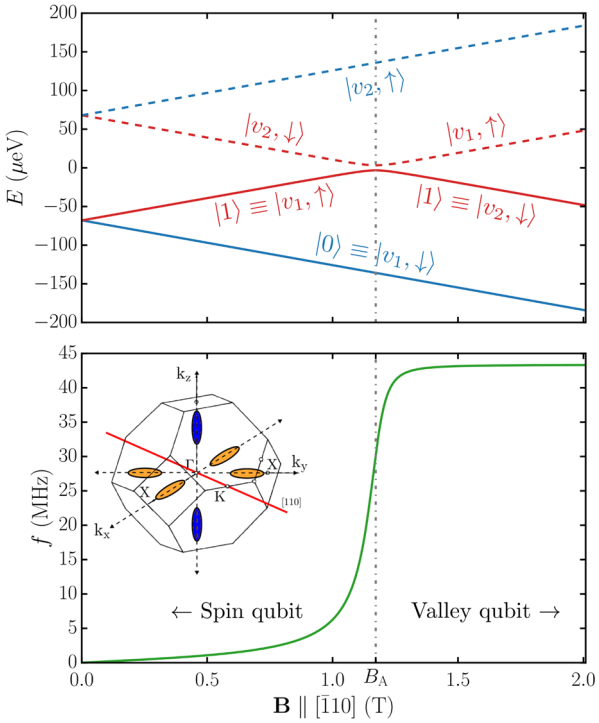

Figure 5: (top panel) Single-particle energy levels in the conduction band of a thin Si quantum dot (see Fig. 3) as a function of the magnetic field. At zero field, the degeneracy between the ±Z valleys (inset of bottom panel) is lifted by steep confinement at the Si/SiO_2 interface; the resulting v_1 and v_2 states are further split by the Zeeman interaction at finite magnetic field. The $|v_1,\uparrow\rangle$ state anti-crosses the $|v_2,\downarrow\rangle$ state around $B = B_A$ due to SOC; This enables electrically-driven Rabi oscillations between the lowest two states $|0\rangle$ and $|1\rangle$ as the electric dipole matrix element between $|v_1,\downarrow\rangle$ and $|v_2,\downarrow\rangle$ is finite. The calculated Rabi frequency is plotted in the lower panel (amplitude of the RF signal on the gate V_{RF} = 1mV). Adapted from [16].

manipulation of the spin by RF electric fields, and hinders the electrical tuning of the gyromagnetic factor g and Zeeman splitting ΔE that may be used to put spins in or out of resonance with a global RF magnetic field in order to address a particular qubit [21].

Yet recent experiments have shown that SOC can be sizable in electron qubits. Ref. [11] for example has demonstrated clear fingerprints of electric dipole spin resonance (EDSR), that is of electrically driven spin rotations, in a device similar to Fig. 1. Detailed microscopic modeling unveiled the mechanisms at play in this device [11].

The EDSR actually results from the interplay between spin and valley physics. Indeed, the X/Y/Z conduction band valleys are sixfold degenerate in bulk silicon [22]. Weak confinement in an anisotropic quantum dot such as those of Figs. 1 and 3 rises the X and Y valleys with respect to the ground-state Z valleys. Strong confinement at the steep Si/SiO_2 interface further couples the +Z and −Z valleys, leaving two valley states v_1 and v_2 at low energy split by a valley splitting energy Δ, which can range from a few tens to a few hundreds of μeV depending on the vertical electric field.

Under a finite magnetic field, the $|v_1,\downarrow\rangle$ and $|v_2,\downarrow\rangle$ states go down in energy, while $|v_1,\uparrow\rangle$ and $|v_2,\uparrow\rangle$ go up (Fig. 5). At some critical field B_A, $|v_1,\uparrow\rangle$ and $|v_2,\downarrow\rangle$ cross and get mixed by SOC. Near the anti-crossing point, the $|v_1,\uparrow\rangle$ state admixes a significant fraction of $|v_2,\downarrow\rangle$. Since $|v_1,\uparrow\rangle$ and $|v_2,\downarrow\rangle$ can be coupled by an electric field, this allows for electrically

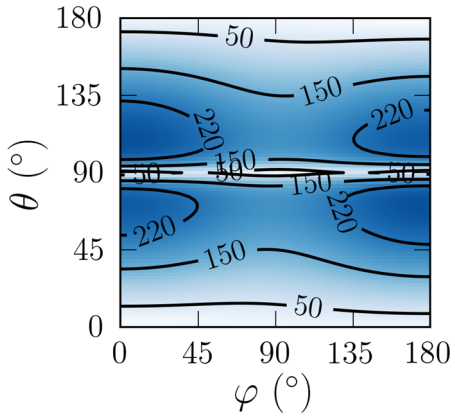

Figure 6: Map of the Rabi frequency (number of spin rotations per second, in MHz) of a heavy-hole spin qubit as a function of the orientation of the magnetic field, characterized by the angles θ and φ (see definition and device on Fig. 3) [13, 23]. The amplitude of the RF signal driving the rotations is V_{RF} = 1mV and the magnitude of the magnetic field is B = 1T (the Rabi frequency being proportional to V_{RF} and B).

driven rotations between the lowest two qubit states. The resulting Rabi frequency is plotted as a function of the magnetic field in the lower panel of Fig. 5. The Rabi frequency saturates beyond the anti-crossing point as the device becomes a "valley" qubit where the information is encoded into the valley states $|v_1,\downarrow\rangle$ and $|v_2,\downarrow\rangle$. Such a valley qubit is, however, very sensitive to charge noise.

SOC is enhanced by the very low symmetry of the "corner dots" formed in SOI devices (Fig. 3). We have demonstrated that the valley splitting and the SOC can actually be tailored by front and back-gate electric fields; and have proposed a manipulation scheme where an almost pure spin qubit (well protected from charge noise but hardly controllable electrically) can be transformed back and forth into a spin-valley qubit (or even a pure valley qubit) for fast electrical manipulation [16].

B. Hole spin qubits.

The physics of holes is very different yet extremely rich [10, 13]. There is no valley degree of freedom, but a strong interplay betwen heavy- and light-holes instead. The mixing between heavy- and light-hole envelopes in the quantum dot is actually a pre-requisite for the electrical manipulation of hole "spins". Since SOC is much stronger in the valence than in the conduction band, electrical driving of hole spins can be very efficient, with Rabi frequencies reaching a few tens of MHz [9, 10].

The linear response of hole spins to magnetic and electric fields can be described in a unified framework based on a gyromagnetic g-matrix and on its derivative with respect to the gate voltage [10, 13]. This g-matrix formalism can be used to analyze experimental data and to model spin qubits at a very low computational cost (Fig. 6). The figures of merit of holes, such as the Zeeman splittings and Rabi frequencies, show a much stronger dependence on the orientation of the fields than those of electrons – a fingerprint of the above-mentioned interplay between the heavy- and light-hole components. This can provide additional control knobs on the hole qubits, but may also enhance variability, and therefore calls for a careful design of the devices.

We have shown that silicon provides excellent opportunities for fast hole spin manipulation owing to its very anisotropic valence band that favors heavy- and light-hole mixing [23, 24]. We have also analyzed the response of hole spin qubits to strains [13, 23]. Semiconductor spin qubits in general tend to be very responsive to strains due to the small energy scales involved in these devices [25, 26].

V. Conclusions

We have discussed the modeling of silicon spin qubits derived from MOS technologies. While CMOS modeling usually focuses on transport at room temperature in the high carrier density regime, spin qubits are operated in the opposite, few electrons and very low temperature limit. Therefore, the methods and tools needed to address qubit devices are different from those used for conventional CMOS; yet they can leverage on the knowledge brought by CMOS modeling on, e.g., disorder and scattering in MOS devices.

We have illustrated the relevance of modeling on a few examples dealing with the electrical manipulation of electron and hole spins. Modeling of decoherence, spin readout, and two-qubit gates will provide in the near future a more complete picture of the expected strengths and weaknesses of silicon qubits with respect to competing technologies. Modeling will also certainly play a leading role in assessing the variability of silicon qubit devices [16, 19].

Acknowledgment

This work was supported by the French ANR project MAQSi and the EU H2020 project MOSQUITO.

References

[1] T. D. Ladd *et al.*, Nature **464**, 45 (2010).
[2] D. Loss and D. P. DiVincenzo, Physical Review A **57**, 120 (1998).
[3] R. Hanson and D. D. Awschalom, Nature **453**, 1043 (2008).
[4] J. J. L. Morton *et al.*, Nature **479**, 345 (2011).
[5] J. Yoneda *et al.*, Nature Nanotechnology **13**, 102 (2018).
[6] T. F. Watson *et al.*, Nature **555**, 633 (2018).
[7] W. Huang *et al.*, Nature **569**, 532 (2019).
[8] A. M. Tyryshkin *et al.*, Nature Materials **11**, 143 (2012).
[9] R. Maurand *et al.*, Nature Communications **7**, 13575 (2016).
[10] A. Crippa *et al.*, Physical Review Letters **120**, 137702 (2018).
[11] A. Corna *et al.*, npj Quantum Information **4**, 6 (2018).
[12] Y.-M. Niquet *et al.*, Physical Review B **79**, 245201 (2009).
[13] B. Venitucci *et al.*, Physical Review B **98**, 155319 (2018).
[14] D. Osintsev *et al.*, Solid-State Electronics **90**, 34 (2013).
[15] B. Voisin *et al.*, Nano Letters **14**, 2094 (2014).
[16] L. Bourdet and Y.-M. Niquet, Physical Review B **97**, 155433 (2018).
[17] C. D. Sherrill and H. F. Schaefer III, Advances in Quantum Chemistry **34**, 143 (1999).
[18] S. Roche and D. Mayou, Physical Review Letters **79**, 2518 (1997).
[19] D. J. Ibberson *et al.*, Applied Physics Letters **113**, 053104 (2018).
[20] R. Li *et al.*, Science Advances **4**, eaar3960 (2018).
[21] M. Veldhorst *et al.*, Nature Nanotechnology **9**, 981 (2014).
[22] F. A. Zwanenburg *et al.*, Review of Modern Physics **85**, 961 (2013).
[23] B. Venitucci and Y.-M. Niquet, Physical Review B **99**, 115317 (2019).
[24] C. Kloeffel, M. J. Rančić and D. Loss, Physical Review B **97**, 235422 (2018).
[25] J. Mansir *et al.*, Physical Review Letters **120**, 167701 (2018).
[26] J. J. Pla *et al.*, Physical Review Applied **9**, 044014 (2018).